Effect of reactive elements on oxidation behaviour of Fe–22Cr–0.5Mn ferritic stainless steel for a solid oxide fuel cell interconnect

Hyung Suk Seo [a], Guangxi Jin [a], Jae Ho Jun [b], Do-Hyeong Kim [b], Kyoo Young Kim [a],*

[a] *Pohang University of Science and Technology, GIFT, San31, Hyoja-Dong, Pohang 790-784, South Korea*
[b] *Pohang Research Institute of Industrial Science and Technology, San 32, Hyoja-Dong, Pohang 790-784, South Korea*

Abstract

Ferritic stainless steel has become a promising material for metallic interconnects for solid oxide fuel cells (SOFCs) operating in an intermediate temperature range (650–800 °C). Ferritic stainless steels containing reactive elements (REs) such as Crofer22APU and ZMG232 have been developed for SOFC interconnects. Nevertheless, the effectiveness of REs on the growth kinetics of the chromia-rich scale that forms on the ferritic stainless steels is not yet well understood. The current study focuses on the investigation of the effect of REs such as Y, Ce and La on the oxidation behaviour and scale properties of Fe–22Cr–0.5Mn stainless steel. The results show that Y is the most effective reactive element for reducing the scale growth kinetics and area-specific resistance of the chromia scale which forms on this stainless steel. The growth kinetics of the chromia-rich scale can be effectively reduced by the dominant segregation of Y at the interface between the oxide scale and alloy substrate, and by the formation of a thin SiO_2 and MnO layer underneath the Cr_2O_3-rich oxide.
© 2008 Elsevier B.V. All rights reserved.

Keywords: Solid oxide fuel cell; Interconnect; Oxidation; Stainless steel; Reactive element; Chromia-rich scale

1. Introduction

The solid oxide fuel cell (SOFC) is a promising power sources. A significant improvement in the recent development of SOFCs is the reduction of its operation temperature from a high temperature range above 800 °C to an intermediate range of 650–800 °C. The reduction in the operation temperature permits the use of metallic interconnects for SOFCs.

The interconnect is one of the most important components in a SOFC stack and enable electrical connection between the anode of one unit cell and the cathode of the neighboring one. They also act as a physical barrier to separate air and fuel. Hence, interconnects must be good electric conductors and exhibit good oxidation resistance in the SOFC operating environment. Ceramic interconnects such as $La_{1-x}(Sr, Ca)_xCrO_3$ have been used in a SOFC system operating above 800 °C; but metallic interconnects such as stainless steel have been included in interconnect research due to the decrease in the operating

temperature to an intermediate range (650–800 °C). Metallic interconnects are easier to fabricate and have higher electronic and thermal conductivity compared with ceramic interconnects. On the other hand, an oxide scale forms on the surface of metallic interconnects at high temperature and this reduces the electric conductivity of the material and thereby SOFC power [1].

Chromia-forming ferritic stainless steels are currently well known as a promising alloy group for SOFC interconnects because an electrically conductive oxide scale forms at high temperature. They are relatively cost-effective and have a thermal expansion coefficient similar to that of other SOFC components. Nevertheless, they have low resistance for Cr_2O_3 evaporation in the SOFC operating environment. Volatile Cr species such as CrO_3 and $CrO_2(OH)_2$ can contaminate the cathode and cause rapid degradation of cell performance [2].

Manganese has been used as an alloying element in several alloys such as Crofer22APU and ZMG232 to increase the electric conductivity of the scale and the stability of chromia-forming alloys. At elevated temperatures, the manganese-containing alloy forms a spinel phase, which improves the electric conductivity and inhibits Cr evaporation [3,4], in an outer layer of the scale. Furthermore, it has been reported that the pres-

* Corresponding author.
  E-mail address: kykim@postech.ac.kr (K.Y. Kim).

Table 1
Chemical composition of Fe–22Cr–xRE alloys (wt.%)

	Fe	C[a]	Cr	Mn	Al	Si	Ti	Ni	Zr	Y	Ce	La
A	Balance	0.02	21.97	0.50	0.21	0.40	–	0.26	0.22	0.06	–	–
B	Balance	0.02	21.97	0.50	0.21	0.40	–	0.26	0.22	–	0.05	–
C	Balance	0.02	21.97	0.50	0.21	0.40	–	0.26	0.22	–	–	0.05

[a] Maximum.

ence of a RE in the alloy can enhance the selective oxidation of chromium, reduce the growth rate of the scale, change the transport mechanism, and increase scale adherence [5]. Most of the alloy candidates for SOFC metallic interconnects contain REs, but the effect of REs on the oxidation process and electrical properties of the metallic interconnect must be understood clearly through a systematic study.

In this study, the oxidation behaviour and electric properties of Fe–22Cr–0.5Mn alloys containing various REs are investigated in an SOFC operating environment. The results are discussed in terms of the distribution of alloying elements near the interface between the oxide scale and the metal substrate.

2. Experimental

2.1. Materials

Fe–22Cr–0.5Mn ferritic stainless steels with various amounts of Y, Ce and La were prepared by arc melting in a pure argon atmosphere. They were heat-treated at 1200 °C for 24 h for homogenizing and annealed at 800 °C for 1 h. To determine the chemical composition of materials, inductively coupled plasma (ICP) analysis was performed on the specimens. The chemical composition of each specimen is presented in Table 1. Steel A, Steel B and Steel C each contain 0.05–0.06 wt.% Y, Ce and La, and the alloy compositions for all specimens are the same except for the RE.

2.2. Oxidation experiments

For oxidation studies, samples were cut into 20 mm × 10 mm × 2 mm plates, and the surface was polished with grit paper and a diamond suspension up to 1 μm. The samples were oxidized at 800 °C in air in a box furnace for 100–200 h.

2.3. Electrical properties

Samples of 10 mm × 10 mm × 2 mm were ground up to P2000 grit and oxidized for 100 h at 800 °C in air to measure the electric resistance of the scale. The electrical resistance of an oxidized specimen is usually measured in terms of the area-specific resistance (ASR) since the exact thickness of the oxide formed on the metallic surface is difficult to determine [6]. The electrical resistance was measured by a two-probe, four-point ac impedance method. Pt-paste electrodes were applied to the surface of the oxidized alloys while the measurements were conducted in an Ar atmosphere. The resistance was evaluated in terms of the ASR, and the activation energy of electric resistance

was calculated using the following equation [7]:

$$\frac{ASR}{T} = A \exp\left(\frac{E_a}{T}\right) \tag{1}$$

2.4. Analysis of scale alloy

The oxide phases formed on the alloy surface for 200 h at 800 °C in air were analyzed by means of X-ray diffraction. A cross-section of the scale was examined by scanning electron microscopy (SEM) and an electron probe microanalyzer (EPMA). The distribution of major and minor alloying elements was analyzed by secondary ion mass spectrometry (SIMS: CAMECA ims-6f) and glow discharge optical emission spectrometry (GDS: LECO 850A) in its depth profile mode. For SIMS, the primary O_2^+ beam sputtered the sample surface, and M^+ secondary ions were collected as a function of sputter time (depth from the surface) over an area of 200 μm² (M^+: each metal species; acceleration voltage: 12.5 kV; primary beam intensity: 1 μA). For GDS, Ar sputtering was performed and the depth profiles were measured over an area of 2 mm in diameter.

3. Results

3.1. Phase identification and microstructure of oxide scale|alloy interface

The XRD patterns of the oxide scales formed on Steels A–C after 200 h of oxidation are shown in Fig. 1. Spinels of Mn–Cr type are marked as 'S', the Cr_2O_3 phase as 'C' and the alloy phase as 'A'. The oxide scales developed on all three steels consist mainly of Cr_2O_3 and Mn–Cr type spinel.

Fig. 2 presents cross-sectional microstructures of the oxide scale|alloy interface. It is shown that the thickness of the oxide scale is highest for Steel B and that all the oxide scales have three different colour contrasts: gray on top, bright in the middle and dark at the bottom. Identification of each phase of the oxide scale was carried out by means of EPMA and GDS analyses, which will be further discussed in a later section. The dark precipitations of internal oxide on Steels A–C are identified as Al_2O_3. The internal oxide appears to be less active in Steel A than in the other specimens. This suggests that the addition of Y suppresses effectively the formation of internal oxide.

The EPMA analyses on all steels are given in Fig. 3. The distributions of element in Steels A–C are similar, and the element mappings show that oxygen is present both in the oxide scale and in the internal oxide precipitation regions. Manganese was present at the outermost oxide surface layer with O and Cr contents. These results suggest that the outermost layer of the oxide
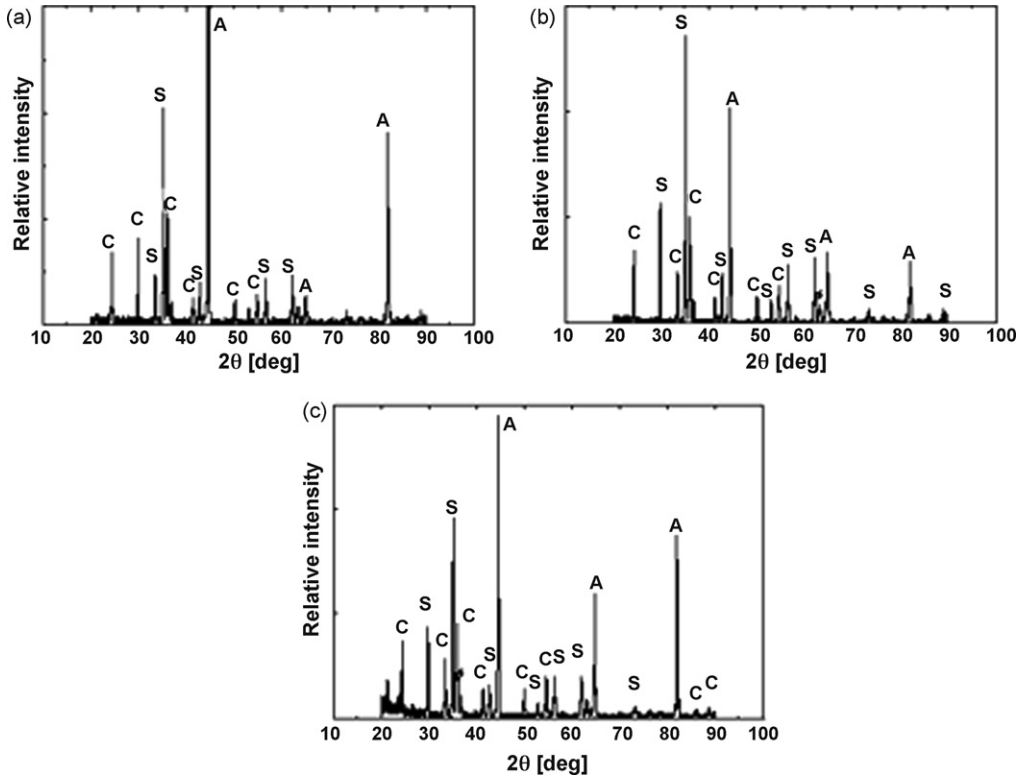
Fig. 1. XRD patterns for oxide phase: (a) Steel A; (b) Steel B; (c) Steel C.

scale is composed of a Mn–Cr type spinel. Silicon is present continuously on the bottom of the oxide scale, and it matches with the dark bottom part as shown in Fig. 2 indicating that a thin Si oxide layer forms on top of the alloy substrate. Moreover, between the Si oxide layer on the bottom and the spinel on the top layer, a dominant Cr signal is observed and indicates that this layer is composed mainly of Cr_2O_3.

The gray portion of the scale shown in Fig. 2 is identified as a combination of Mn–Cr type spinel and Cr_2O_3-rich oxide. A narrow distribution of Mn is observed along with Fe between the
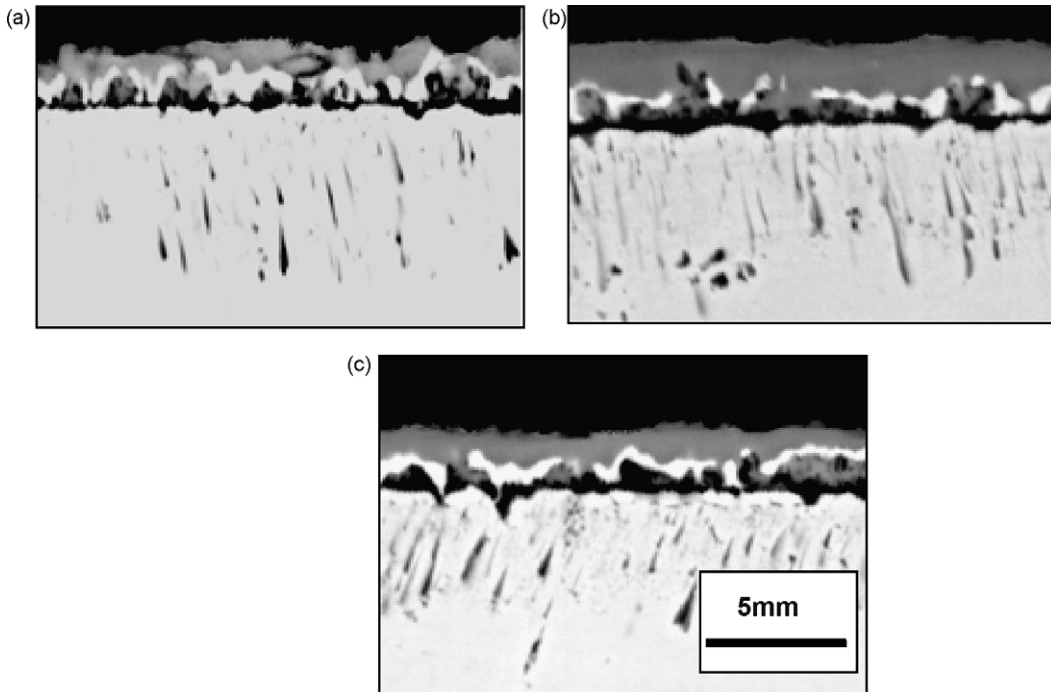

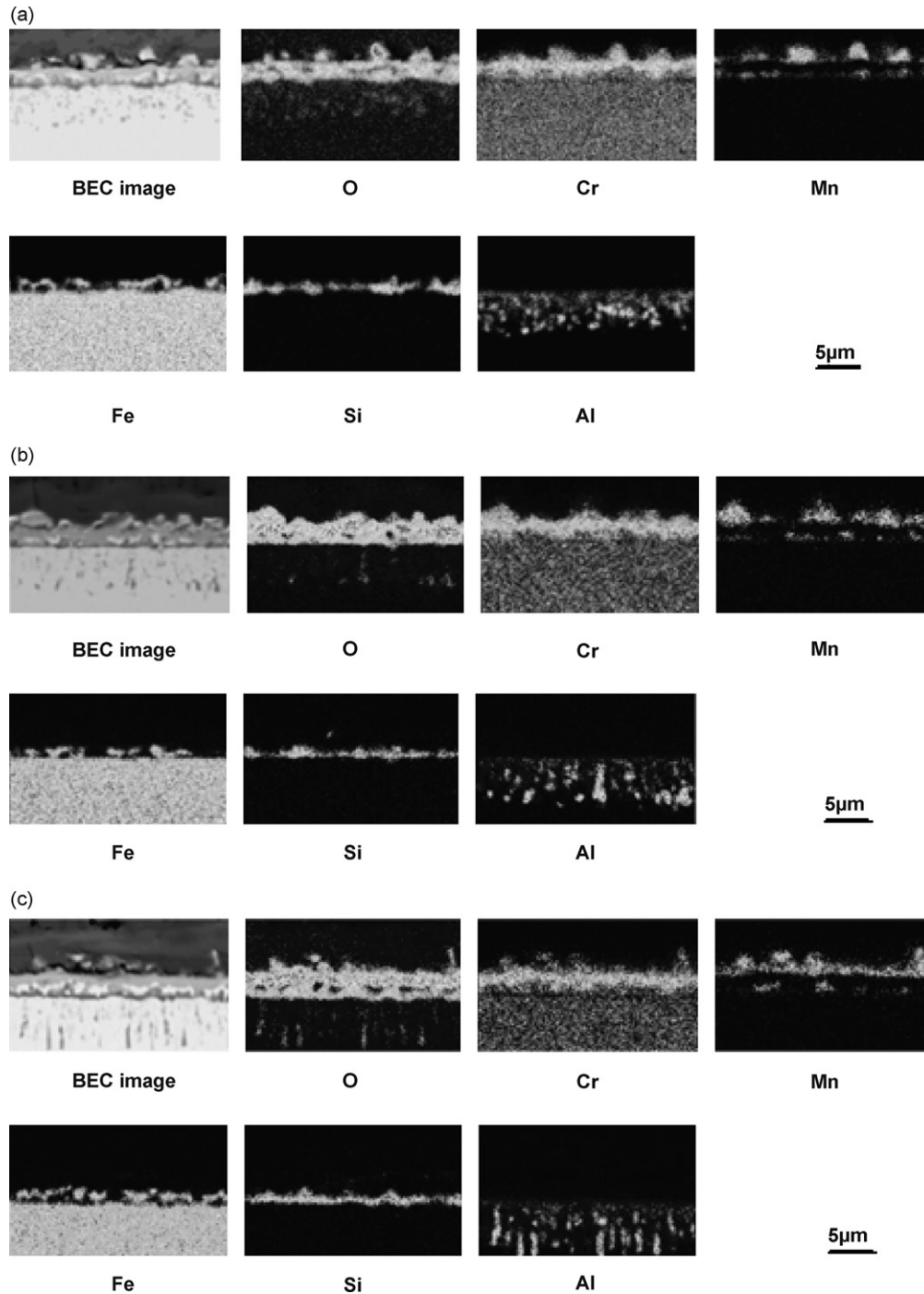Fig. 2. Microstructure of oxide scale|alloy interface: (a) Steel A; (b) Steel B; (c) Steel C.

Fig. 3. EPMA analysis: (a) Steel A; (b) Steel B; (c) Steel C.

bottom portion of the Cr-dominant region and the upper portion of the Si oxide layer. This suggests that Mn–Fe–Cr type spinel and/or Fe–Cr type spinel is formed in the intermediate region (bright zone) of the oxide scale. It is believed that the presence of Fe in the spinel improves electric conductivity at elevated temperature [8]. Discontinuous distribution of the bright zone may not, however, contribute significantly to the improvement of the electric conductivity of the scale. The distribution of Al and O is in good agreement with the microscopic images shown in Fig. 3. The presence of other minor elements such as Zr and

RE is difficult to identify due to the small amounts present in the steel.

3.2. GDS and SIMS analysis

Fig. 4 shows the GDS depth profiles of reactive elements present near the interface between the oxide scale and alloy. The interface region of the oxide and alloy are divided into three regions: X for the outermost oxide surface, Y for the main body of oxide, and Z for the alloy substrate. The region X is an out-
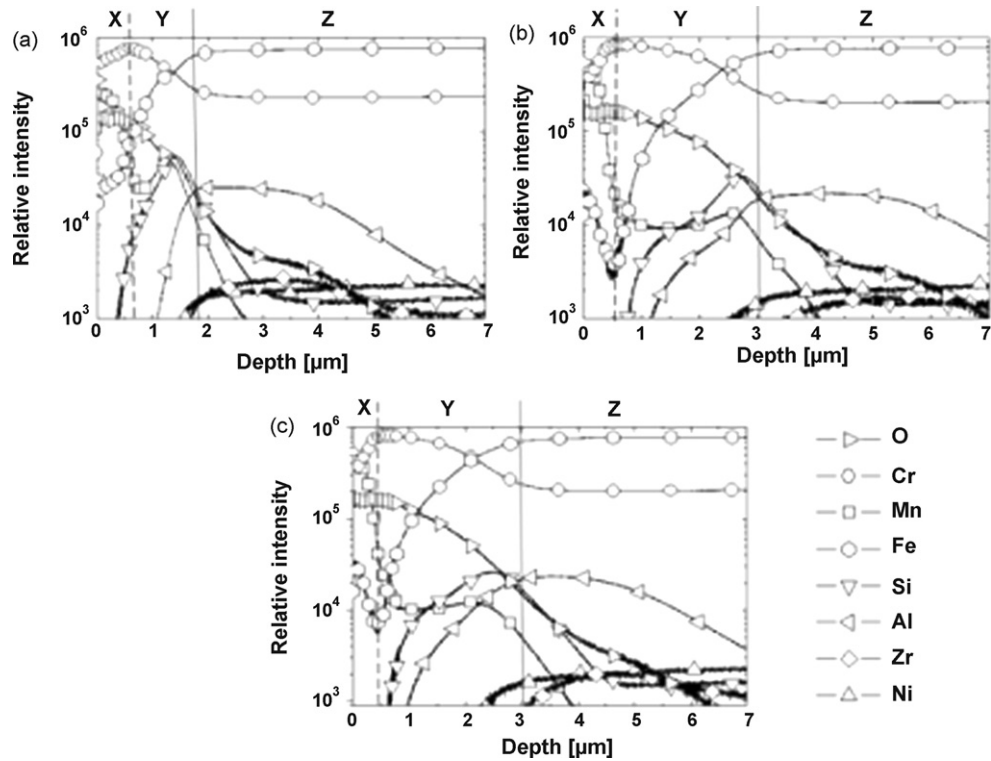
Fig. 4. GDS depth profile of elements near interface between oxide scale and alloy: (a) Steel A; (b) Steel B; (c) Steel C.

ermost spinel part where Mn and Cr are enriched. Below the spinel, Mn content decreases rapidly and Cr becomes dominant in the outer part of region Y. This is an indication that Cr_2O_3 forms mainly in this region. In the lower side of region Y, the Cr content decreases as it moves from the oxide to the alloy. A strong Si peak is observed in Steels A–C, in which Si oxide is observed on top portion of the steel substrate. The GDS profile suggests that the oxide scale corresponds to regions X and Y, and region Z corresponds to the alloy substrate with internal oxide. Al is enriched in the alloy underneath the oxide scale and rapidly decreases in concentration in the oxide scale. The low diffusion characteristics of Al in the scale are demonstrated in Fig. 4. Thus, the interface between the alloy and the oxide scale can be determined by detecting the point at which the Al content starts to decrease just below the point where the Si peak is the highest. In this paper, the oxide thickness was measured by the distance from the oxide scale surface to the point where Al starts to decrease just below the highest Si peak point.

The GDS depth profile result is in a good agreement with EPMA and SEM results; consequently, the microstructure of the oxide scale is identified from these results. In all steels, the Mn–Cr spinel forms at the outermost surface of the oxide scale. A Cr_2O_3-rich layer forms widely underneath the spinel layer but the thickness and uniformity of this layer varies depending on the steel composition, particularly on the type and amount of a reactive element. The point where the Si peak is the highest corresponds to the secondary peak point of Mn near the interface between the oxide scale and alloy. This indicates that a mixed oxide of Mn–Si develops on top of the alloy substrate. Underneath the oxide scale, internal oxidation of Al in the alloy can

be clearly identified by observing the Al profile. The spinel layers in Steels A–C have similar thickness. On the other hand, the Cr_2O_3-rich layer on Steel A is significantly thinner than the rest.

The above observation is supported by Horita et al. [9] who explained the possibility of forming thin Si and Mn oxide layers beneath the Cr_2O_3-rich layer near the interface between the oxide scale and the alloy. Assuming the activity of the metal is constant, the value of equilibrium oxygen partial pressure, $P(O_2)$, is 1.1×10^{-30} Pa for SiO_2, 1.6×10^{-25} Pa for MnO, 1.9×10^{-20} Pa for Mn_3O_4, and 1.4×10^{-23} Pa for Cr_2O_3. The oxygen partial pressure of the scale decreases towards the alloy side from the oxide surface. If the oxygen partial pressure is lower than the equilibrium partial pressure of Cr_2O_3, Cr_2O_3 cannot be produced and an oxide with a lower equilibrium oxygen partial pressure such as SiO_2 and MnO can form. In this case, the oxidation occurs at the oxide scale|alloy interface by inward diffusion of oxygen.

Minor elements such as REs are difficult to detect due to their low concentration when GDS analysis is used. Thus, SIMS is used to obtain the distribution of REs as shown in Fig. 5. The data show reactive element distribution near the interface between the oxide scale and the alloy. For Steel A containing 0.06 wt.% Y, the profile shows that Y is enriched at the interface between the oxide scale and the alloy and this suggests that diffusion in the oxide is slow even though diffusion of Y in the alloy is fast. It is believed that Y concentrated near the interface may enhance the adhesion of the scale to the metal and improve the stability of the oxide. For Steel B containing 0.05 wt.% Ce, the profile of Ce is fairly constant throughout the interface between the oxide scale and the alloy. It decreases toward the scale surface, however, and
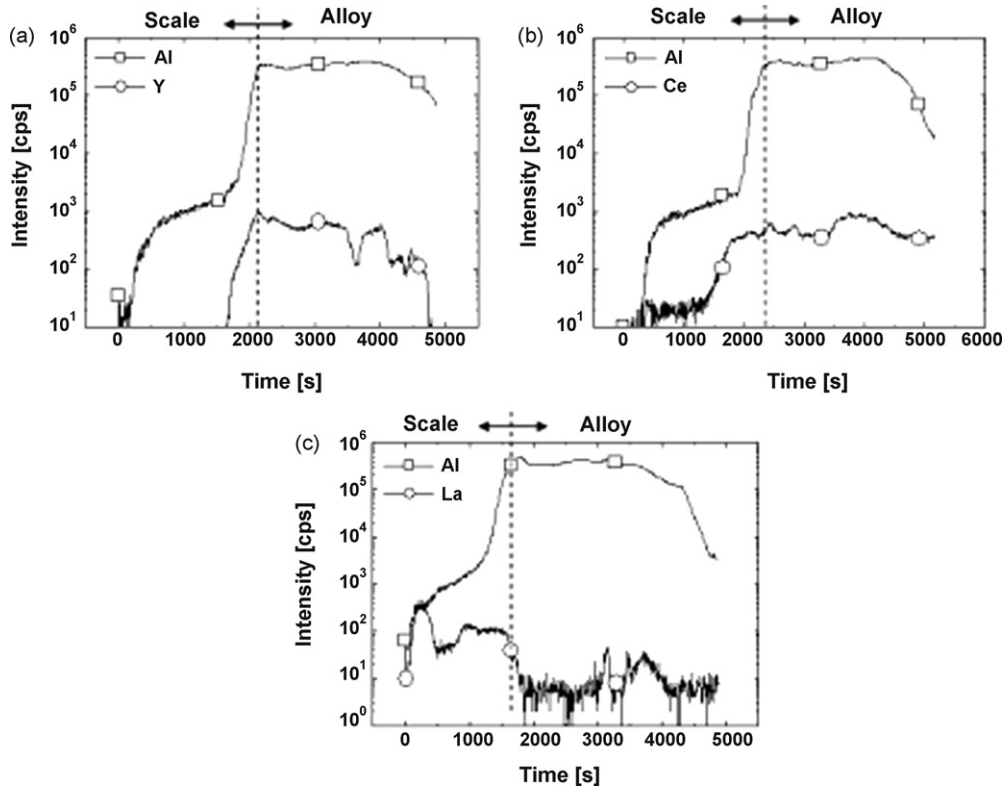
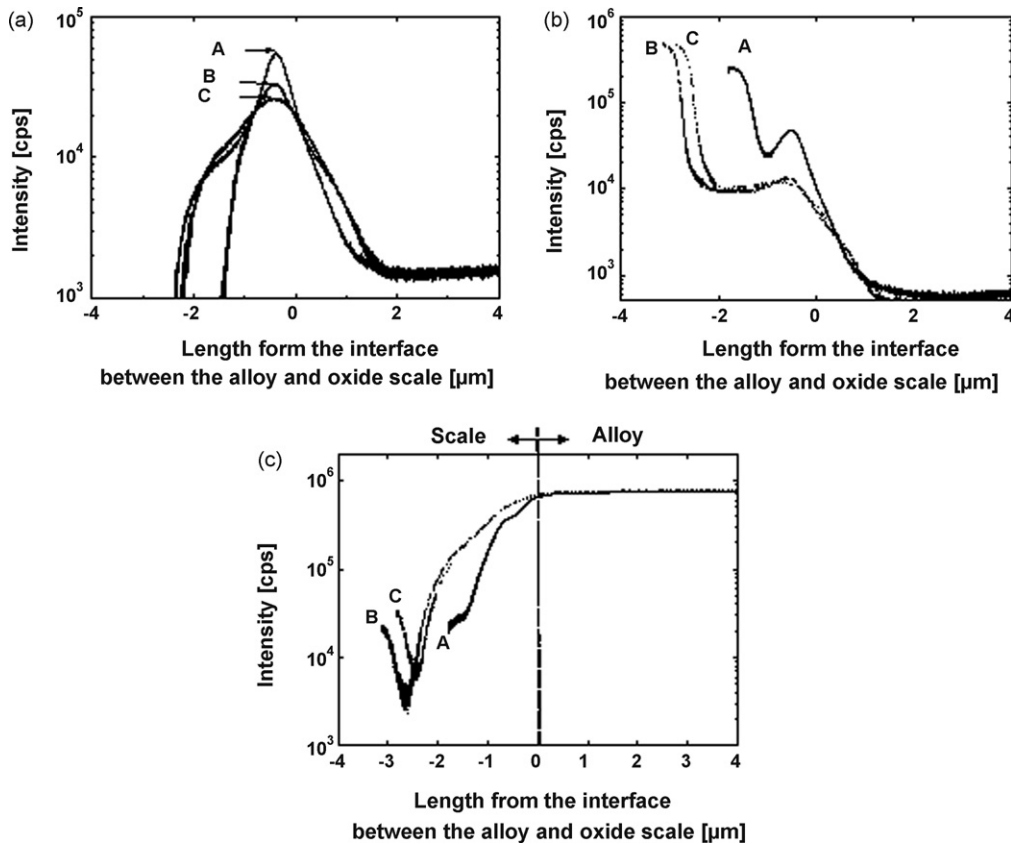Fig. 5. Depth profiles of reactive element in (a) Steel A; (b) Steel B; (c) Steel C.

Fig. 6. Comparison of GDS data for elemental distribution in different steels: (a) Si distribution; (b) Mn distribution; (c) Fe distribution.

Table 2
Activation energy and growth rate constant of various experimental steels

	A	B	C
E_a (eV)	0.85	0.76	0.75
k_p ($\mu m^2\,s^{-1}$)	4.52×10^{-6}	1.34×10^{-5}	1.13×10^{-5}

the concentration of Ce near the oxide|alloy interface is lower than that of Y. For Steel C containing 0.05 wt.% La, the profile shows that La is enriched at the oxide scale and is depleted below the oxide scale. Furthermore, the diffusion of La in the oxide scale is faster than that of Y and Ce. La may exist in two forms: La-oxide incorporated in Cr_2O_3 and Si–Mn oxide and La-oxide precipitated along the grain boundaries of the oxide scale. The La–Cr type oxide has a relatively low electric resistance [10], i.e., it contributes to an increase in the electric conductivity of the scale. The concentration of La near the interface between the oxide scale and the alloy is lower than that of Y and Ce.

These differences in RE distribution near the oxide scale|alloy interface significantly affect the oxidation behaviour. Fig. 6 shows the distribution of Si, Fe and Mn in the oxide scale. The inner Si peak of Steel A near the oxide scale|alloy interface is relatively higher than that of Steels B and C, but the Si oxide band in Steel A is thinner than that in other steels. A comparison between Fig. 6(a) and (b) indicates that the profile of the secondary Mn peak corresponds to that of the Si peak, as observed from the GDS profiles shown in Fig. 4. The Fe peak of Steel A decreases more rapidly compared with those of Steels B and C. These distribution differences can be explained by the type and distribution of the reactive element (RE) near the oxide scale|alloy interface. This will be discussed in detail later.

3.3. Oxide scale property

The ASR of each oxide scale was measured and the results are shown in Fig. 7(a). Steel A containing 0.06 wt.% Y shows the lowest values of ASR under the experimental conditions. The activation energies of the three steels were obtained from ASR data of the oxide scale and are reported in Table 2. They are in a range of 0.75–0.85 eV.

Fig. 7(b) shows the change in oxide scale thickness with oxidation time tested at 800 °C in ambient air. The oxidation behaviour of all three steels follows well the parabolic rate equation:

$$X^2 = k_p t \tag{2}$$

The values of the growth rate constant, k_p, are given in Table 2. The growth rate of Steel A is slower than that of Steels B and C. This suggests that the addition of Y is more effective in reducing the oxide scale growth than that of La and Ce for a given alloy condition.

4. Discussion

Steels A–C have a similar oxide scale structure which is composed of a Mn–Cr type spinel on the outermost scale surface that is mixed with a Cr_2O_3-rich oxide (gray zone), an intermediate
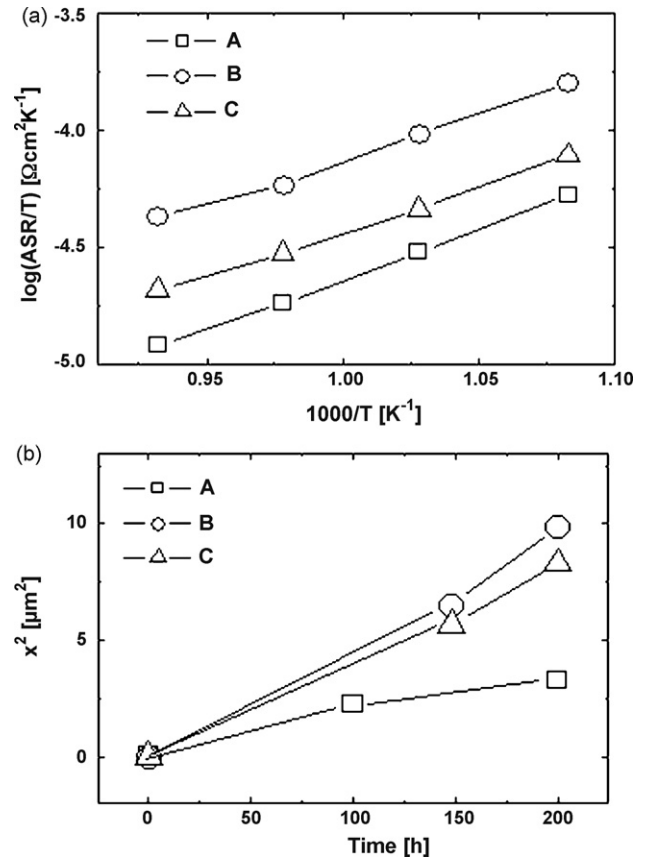

Fig. 7. (a) Area-specific resistance of each oxide scale and (b) oxide scale growth behaviour.

Mn–Cr–Fe spinel and/or a Cr–Fe spinel (bright zone), and a mixed oxide of Si–Mn–Fe on the innermost (dark zone). However, the oxidation growth rate and the element distribution in the oxide scale are strongly dependent on the type of RE. The oxide scale growth kinetics are primarily expressed by a parabolic rate law. It is clear that a RE affects the diffusion process, resulting in a different structure of the oxide scale.

The examination of SIMS data shows that Y is mainly concentrated along the interface between the alloy and oxide layer. The segregation of reactive elements at the oxide|alloy interface stops cation vacancy annihilation; thus, cation transport through the scale is depressed [5,11]. As a result, anion transport becomes the dominant diffusion process, and the oxidation site changes from the gas|oxide interface to oxide|alloy interface. Such an effect by the RE is manifested strongly in Steel A due to the Y segregation at the interface between the oxide and the alloy. By contrast, this effect is relatively weak in Steel B because Ce segregation is dispersed farther into the oxide scale. A comparison of Fig. 6(a) and (b) indicates that the formation of SiO_2, and MnO is more effectively suppressed in Steel A than in Steels B and C. This result clearly shows that the Y segregation along the oxide|alloy interface depresses the outward diffusion of the cations more effectively in Steel A than in Steels B and C.

La spreads throughout the entire oxide scale and its addition may not effectively stop cation vacancy annihilation near the oxide|alloy interface. A different mechanism is proposed to

explain the effect of the RE on oxide growth. It is proposed that the segregation of RE along the oxide grain boundaries greatly retards cation outward transport through the scale [5,12]. Thus, La in Steel C also reduces outward diffusion of cations and renders inward anion transport dominant.

In the case of Y segregation along the alloy|scale interface, cations cannot diffuse out easily since Y segregation can effectively block outward diffusion through the interface by stopping vacancy annihilation. On the other hand, in the case of La segregation along the grain boundaries of the oxide scale, some cations could diffuse out through the alloy|scale interface since La does not block the interface completely, but blocks only along the scale grain boundaries. For this reason, it is possible for Si to diffuse farther out in the oxide scale in Steel C than in Steel A. Therefore, the SiO$_2$ formed on Steel A has a thin but a continuous layer along the alloy|scale interface as shown in Fig. 2(a), whereas SiO$_2$ formed on Steel C has a thick and irregular shaped layer with protrusions into the scale as shown in Fig. 2(c). To explain the outward diffusion behaviour of Mn and Fe as observed in Fig. 6, the same effect of Y and La can be applied. Therefore, Y and La reduce the oxidation growth rate by depression of the outward diffusion of cations, but with entirely different mechanisms.

The partial pressure of oxygen in the area underneath Cr$_2$O$_3$ falls below 1.4×10^{-23} Pa; thus, the only possible elements to develop an oxide are Si and Mn, as SiO$_2$ and MnO, respectively [9]. The Y segregation along the scale|alloy interface suppresses cation diffusion, and causes Si and Mn to oxidize locally at the scale|alloy interface. As a result, the formation of SiO$_2$ and MnO in Steel A is more compact and intensive than in other steels along the scale|alloy interface as shown in Figs. 2 and 6(a). These compact SiO$_2$ and MnO oxide layers can block diffusion of ions and suppress the oxidation rate.

Steel A containing 0.05 wt.% Y has the lowest ASR value. Y is known to suppress ion transport while it has no effect on the electron transport in chromia [9]. Also, Y improves the scale adherence of chromia [5]. The Y-rich oxide layer at the alloy|scale interface suppresses ion diffusion for the scale growth; consequently, it reduces the scale growth rate. As a result, the path for electric conduction becomes short due to a thin oxide layer, and the scale has a low electric resistance since the ASR of one side of specimen is defined as [13]:

$$ASR = RA = \rho_o l_o \tag{2}$$

where R is the resistance; A the surface area; ρ_o the resistivity; l_o

is the thickness of the oxide layer. The oxide layer thickness, l, formed on the alloy cannot be exclusively determined. According to the data obtained from SEM, EPMA, GDS and SIMS, the overall effectiveness of a RE on the kinetics of chromia-forming ferritic stainless steel is of the order of Y > La > Ce for a given alloy composition (RE excluded).

5. Summary

The effect of REs such as Y, Ce and La on the oxidation behaviour and scale properties on Fe–22Cr–0.5Mn stainless steel have been investigated. The results are discussed in terms of distribution of alloying elements across the oxide scale to enhance the understanding of the effectiveness of a RE on the growth kinetics of chromia-forming oxide and the area-specific resistance of the oxide scale. The results are summarized as follows.

(1) Y is the most effective RE for reducing the scale growth kinetics as well as the area-specific resistance of the chromia scale formed on Fe–22Cr–0.5Mn stainless steel.
(2) Growth kinetics of chromia-rich scale can be effectively reduced by the dominant segregation of Y along the alloy|scale interface and by the formation of a compact SiO$_2$ and MnO layer beneath the Cr$_2$O$_3$-rich oxide.
(3) The major role of REs is to make the oxidation process of chromia-rich scale the dominant inward diffusion of anions. Its mechanism, however, may be different depending on the type and amount of REs.

References

[1] S.C. Singhal, K. Kendall (Eds.), High Temperature Solid Oxide Fuel Cells, Elsevier Advanced Technology, New York, 2003.
[2] H. Tu, U. Stimming, J. Power Sources 127 (2004) 284.
[3] P. Kofstad, High Temperature Corrosion, Elsevier, New York, 1988.
[4] Z.G. Lu, J.H. Zhu, E.A. Payzant, M.P. Paranthaman, J. Am. Ceram. Soc. 88 (2005) 1050.
[5] P.Y. Hou, J. Stringer, Mater. Sci. Eng. A 202 (1995) 1.
[7] S.J. Geng, et al., Solid State Ionics 177 (2006) 559.
[6] T. Horita, et al., J. Power Sources 131 (2004) 293.
[8] N. Sakai, et al., Solid State Ionics 176 (2005) 681.
[9] T. Horita, et al., J. Power Sources 157 (2006) 681.
[10] H. Taguchi, et al., Physica B 270 (1999) 325331.
[11] R.A. Rapp, B. Pieraggi, J. Electrochem. Soc. 140 (1993) 2844.
[12] G.M. Ecer, G.H. Meier, Oxide. Met. 159 (1979) 13.
[13] W.Z. Zhu, S.C. Deevi, Mater. Res. Bull. 38 (2003) 957.